MULTIPHASE TRANSPORT AND PARTICULATE PHENOMENA

VOLUME 1

Edited by

T. Nejat Veziroğlu
Clean Energy Research Institute
University of Miami

HEMISPHERE PUBLISHING CORPORATION
A member of the Taylor & Francis Group
New York Washington Philadelphia London

MULTIPHASE TRANSPORT AND PARTICULATE PHENOMENA: Volume 1

Cover design by Sharon DePass.

1 2 3 4 5 6 7 8 9 0 EBEB 8 9 8 7 6 5 4 3 2 1 0 9

Library of Congress Cataloging-in-Publication Data

Multiphase transport and particulate phenomena / edited by T. Nejat Veziroğlu.
p. cm.
Papers presented at the 5th Miami International Symposium on Multiphase Transport and Particulate Phenomena.

1. Multiphase flow—Congresses. 2. Heat—Transmission—Congresses. 3. Mass transfer—Congresses. I. Veziroğlu, T. Nejat. II. Miami International Symposium on Multiphase Transport and Particulate Phenomena (5th)
TA357.M85 1990
620.1'064—dc20 80-19776
CIP

ISBN 1-56032-026-5 (set)
ISBN 1-56032-030-3 (Vol. 1)

Contents

[9] Rodi, W., "Turbulence Models and Their Application in Hydraulics", AIHR Monograph (1984).

[10] Andritsos, N. and Hanratty, T.J., "Influence of Interfacial Waves in Stratified Gas-Liquid Flows", AIChE Journal, Vol. 33, No. 3, pp. 444-453, (1987).

[11] Ishii, M. and Zuber, N., "Relative Motion and Interfacial Drag Coefficients in Dispersed Two-Phase Flow of Bubbles, Drops and Particles", AIChE Journal, Vol-25, No. 5 (1979).

[12] Drew, D.A. and Lahey, R.T., Jr., "The Virtual Mass and Lift Force on a Sphere in Rotating and Straining Flow", J. of Multiphase Flow, Vol-13, No. 1, pp. 113-121 (1987).

Turbulence Modeling and Distribution of Phases in an Annular Two-Phase Flow

FLAVIO DOBRAN and NAHMKEON HUR
New York University
Applied Science Department
New York, New York 10003, USA

Abstract

A mixing length turbulence model is used to study the distribution of liquid and gas in the core of an annular two-phase flow. The gas volumetric fraction distributions were obtained for different regions of the core and then combined to obtain the distribution for the entire region. In vertical upflow a peak in the volumetric fraction is predicted close to the liquid film interface for some range of flow parameters, whereas in downflow the peak is predicted at the pipe centerline. Larger interfacial shear stresses have the effect of increasing the gas phase concentration close to the liquid film interface, and larger values of the average void fraction produce more uniform profiles in both upflow and downflow. By comparing the predictions of the model with the upflow and downflow air-water data of different diameter tubes, the turbulence parameters are explicitly identified and it is shown that the model predicts well the data over a wide range of liquid and gas flow-rates.

1. INTRODUCTION

An annular two-phase flow pattern occurs widely in many practical situations and as illustrated in Fig. 1 it consists of a liquid film adjacent to the tube wall and of a gas core region. The interfacial region between the film and gas core is usually not smooth, but instead it may be covered by a complex system of waves which at sufficiently high gas flow-rates break up and some of the liquid becomes entrained in the gas core in the form of liquid droplets. Since the amount of liquid flowing in the core can be considerable, it is reasonable to expect that it can significantly affect the total flow field distribution and evolution. By its very nature, a practical two-phase annular flow pattern is turbulent and in a hydrodynamic nonequilibrium, since it usually requires a large distance in the tube before the local liquid entrainment rate from the film balances the local liquid deposition rate onto the liquid film ([1], chapter 2). Heat and mass transfer further complicate the situation and may have a significant effect on the distribution of liquid in the film, interfacial transfer, and on the distribution of liquid and gas in the core region.

A great deal of effort has been devoted in the past towards the understanding of an annular two-phase flow pattern [1-3]. Most of these studies have been concerned, however, with the global aspects of the flow which require relatively simple instrumentation to gather data for the justification of proposed analytical models. Simple models turn out to be unsatisfactory,

especially for nonequilibrium flows, and a possible means to improve global models is through the studies of local flow characteristics such as the distribution of phases in the core region. The distribution of liquid and gas phases in the core is inherently coupled with the state of the liquid film, direction of the gravity field vector with respect to the flow direction, relative motion of the film and core, external driving force of the flow (pressure gradient), etc. Gill et al. [4,5] experimentally studied the distribution of liquid droplets in the core of an upflowing annular flow and found that the gas volumetric fraction has nearly a flat profile in most of the core region and a very steep gradient near the liquid film interface for a wide range of liquid and gas flow-rates. Near this interface, however, the data from a probe inserted into the flow need a careful interpretation, since the probe may be peaking up liquid from the film surface waves instead from the droplets. The interfacial region of the film and core needs, therefore, to be carefully modeled.

The flow of liquid droplets in the core of an annular flow has some similarity with the dispersed two-phase flows without the liquid film which is easier to study experimentally and to obtain two-phase flow turbulence information that may be used to construct models of annular flows. For this reason, a brief summary of the low quality experimental data of nonannular two-phase flows is of relevance.

Serizawa, Kataoka and Michiyoshi [6] studied the phase distribution and turbulence characteristics of an upflowing bubbly flow and observed the existence of a bubbly layer close to the tube wall at low qualities, whereas at higher qualities the bubbly flow changed to slug flow with a void fraction (volumetric fraction of the gas phase) peak appearing at the center of the tube. In cocurrent downflow, the data of Oshinowo and Charles [7] show no bubble layer close to the tube wall, but instead they show a coring effect where bubbles concentrate near the center of the pipe. Ibragimov et al. [8] also observed a bubbly layer close to the tube wall in upflow and gas coring in downflow. The data of [6] show that the turbulent stress of the gaseous phase is proportional to the liquid phase, and that the two-phase flow turbulence is nearly isotropic. Lance and Bataille [9] observed that the injection of bubbles into an initially quasi-isotropic single-phase turbulent flow field does not change the isotropy of the two-phase flow at low qualities in a vertical rectangular duct. Moreover, the longitudinal turbulent intensity and turbulent kinetic energy increased with an increase of the void fraction. The upflow data of Theofanous and Sullivan [10] show: (1) a bubbly layer near the wall, (2) a substantially isotropic two-phase flow field, and (3) that the bubbles produce an increase in the axial turbulent intensity of the flow. Based on the experimental data of low quality bubbly flows, Drew and Lahey [11] utilized a mixing length model for the turbulent two-phase flow field and qualitatively predicted the experimental void fraction distribution.

Two-phase laminar flows with the dispersed phase being denser than the continuous phase were experimentally investigated for both upflow and downflow by Jeffrey and Pearson [12] who showed that the denser phase migrates to the tube wall for the downward flow and to the axis of the tube for the upward flow. This study, together with the studies involving bubbly flows, illustrates an important conclusion that the gas volumetric fraction has a similar distribution in both upflow and downflow irrespective of whether a lighter or a heavier phase is dispersed in a continuous phase, provided that the gas phase

is being interpreted as the lightest phase in the mixture. Although the flow in the core region of an annular flow is similar to the two-phase flow situation where the denser phase is distributed in a continuous lighter phase, no data appear to exist for this region on the detailed distribution of the gas volumetric fraction.

From the above, it is evident that the core region of an annular two-phase flow needs a more detailed study with the objectives in this paper being: (1) to construct a turbulence model for the core and to use this model to determine the distribution of liquid and gas, and (2) to use the core void fraction model to study the distribution of flow properties in annular flows and test the model predictions with data of vertical upflow and downflow to ascertain the range of validity of the basic turbulence assumptions.

2. TURBULENT FIELD EQUATIONS FOR AN ISOTHERMAL TWO-PHASE FLOW

A study of turbulent flow characteristics of the core region of an annular flow requires a set of turbulent field equations. In this paper this set of equations will be obtained by performing time averaging of the volume-averaged two-phase flow equations developed by Dobran [13,14]. For isothermal and no phase change situations, the conservation of mass and balance of momentum equations of phase k, where k=L denotes the liquid phase and k=G denotes the gas phase, are as follows:

$$\frac{\partial \bar{\rho}_k}{\partial t} + \nabla\cdot\bar{\rho}_k\mathbf{V}_k = 0 \tag{2.1}$$

$$\frac{\partial \bar{\rho}_k\mathbf{V}_k}{\partial t} + \nabla\cdot\bar{\rho}_k\mathbf{V}_k\mathbf{V}_k = \nabla\cdot\mathbf{T}_k + \bar{\rho}_k\mathbf{g} + \mathbf{p}_k \tag{2.2}$$

where $\bar{\rho}_k$ is the partial density of phase k and is defined by

$$\bar{\rho}_k = \alpha_k\rho_k\,, \qquad \alpha_L + \alpha_G = 1 \tag{2.3}$$

In the above equations α_k is the volumetric fraction, ρ_k the density, $\mathbf{T}_k$ the stress tensor, $\mathbf{p}_k$ the momentum interaction[1], and $\mathbf{V}_k$ the velocity of phase k. The gravity vector is denoted by $\mathbf{g}$ and time by t. The volume averaging approach assigns at each point in space and time several mixture properties similar to the modeling of single-phase multicomponent mixtures. Dobran [13, 15] performed a linearized analysis of the constitutive equations and argued that two-phase flows with low volumetric fractions of the dispersed phase have constitutive equations for the stress tensor $\mathbf{T}_k$ and momentum interaction $\mathbf{p}_k$ of the following forms:

$$\mathbf{T}_k = -\alpha_k P_k\mathbf{I} + \lambda_{kk}(\mathrm{tr}\mathbf{D}_k)\mathbf{I} + 2\mu_{kk}\mathbf{D}_k \tag{2.4}$$

$$\mathbf{p}_k = -\varepsilon_{kL}(\mathbf{V}_L-\mathbf{V}_G) - \Delta_{kL}(\grave{\mathbf{V}}_L-\grave{\mathbf{V}}_G)\,, \qquad \mathbf{p}_L + \mathbf{p}_G = \mathbf{o} \tag{2.5}$$

where $\mathbf{D}_k$ is the symmetric part of the velocity gradient, P_k is the pressure, $\grave{\mathbf{V}}_L$

[1] This may include the nonlocal effects [14].

and $\mathbf{v}_G$ are accelerations of liquid and gas, λ_{kk} and μ_{kk} are viscosity coefficients which depend on temperature and densities ρ_L and ρ_G, $\xi_{LL} \geq 0$ and $\xi_{GL} \leq 0$ are drag coefficients, and $\Delta_{LL} \geq 0$ and $\Delta_{GL} \leq 0$ are virtual mass coefficients. In the following, the form of these coefficients is not important, since (2.4) will be rewritten as follows

$$\mathbf{T}_k = -\alpha_k P_k \mathbf{I} + \alpha_k \tau_k \tag{2.6}$$

where τ_k accounts for viscous contributions due to $\mathbf{D}_k$.

To determine the turbulent counterpart of (2.1) and (2.2) we can proceed in the usual way by time averaging these equations over a time interval T that is larger that the time scale of turbulent fluctuations while smaller than the time interval associated with the transient behavior of flow. A time average of a physical variable A, which is a function of space coordinate x and time t, will be defined as folows:

$$\overline{A(x,t)}^T = \frac{1}{T}\int_0^T A(x,t+\tau)\, d\tau \tag{2.7}$$

and used to reduce (2.1) and (2.2) after time averaging. To simplify the resulting set of time-averaged equations it will be assumed that both phases can be represented by the quasi-steady densities ρ_L and ρ_G, and pressures[2], i.e.

$$\bar{\rho}_L^T = \rho_L \,, \qquad \bar{\rho}_G^T = \rho_G \tag{2.8}$$

$$\bar{P}_L^T = \bar{P}_G^T = P \tag{2.9}$$

Denoting by $\mathbf{v}_k$ the turbulent velocity fluctuations and by ϕ_k the turbulent volumetric fraction fluctuations we have

$$\mathbf{V}_k = \bar{\mathbf{V}}_k^T + \mathbf{v}_k \tag{2.10}$$

$$\alpha_k = \bar{\alpha}_k^T + \phi_k \tag{2.11}$$

and note that $\bar{\mathbf{v}}_k^T = \mathbf{0}$ and $\bar{\phi}_k^T = 0$ by definition. Performing time averaging of (2.1) and (2.2) and using (2.7)-(2.11) gives the time-averaged mass and momentum equations, i.e.

$$\frac{\partial}{\partial t}\rho_k \bar{\alpha}_k^T + \nabla\cdot\rho_k(\bar{\alpha}_k^T\bar{\mathbf{V}}_k^T + \overline{\phi_k \mathbf{v}_k}^T) = 0 \tag{2.12}$$

$$\frac{\partial}{\partial t}\rho_k(\bar{\alpha}_k^T\bar{\mathbf{V}}_k^T + \overline{\phi_k \mathbf{v}_k}^T) + \nabla\cdot\rho_k\bar{\alpha}_k^T\bar{\mathbf{V}}_k^T\bar{\mathbf{V}}_k^T = -\nabla(\bar{\alpha}_k^T P) + \nabla\cdot(\bar{\alpha}_k^T\bar{\tau}_k + \bar{\alpha}_k^T\bar{\sigma}_k) + \rho_k\bar{\alpha}_k^T\mathbf{g} + \bar{P}_k^T \tag{2.13}$$

where $\bar{\tau}_k^T$ denotes the viscous contributions of the stress tensor, whereas $\bar{\sigma}_k^T$ denotes the turbulent contributions and includes velocity-velocity and velocity-velocity-volumetric fraction correlations whose forms will not be

[2] This assumption neglects the flow redistribution due to the pressure fluctuations which in single-phase flow can be significant.

separately modeled in the paper and thus will not be listed here.

The distribution of phases in the core region of an annular flow will be studied by the further assumptions of: (1) mean steady flow, (2) fully-developed flow except for the pressure gradient, and (3) axisymmetric flow. By defining $\tau_k = \bar{\tau}_k^T$, $\sigma_k = \bar{\sigma}_k^T$, $\alpha = \bar{\alpha}_k^T$, and utilizing the above assumptions the momentum equation (2.13) is reduced to

Radial momentum equations for the gas and liquid phases:

$$0 = -\alpha\frac{\partial P}{\partial r} + \frac{d}{dr}(\alpha\sigma_{G,rr}) + \frac{1}{r}\alpha(\sigma_{G,rr} - \sigma_{G,\psi\psi}) \tag{2.14}$$

$$0 = -(1-\alpha)\frac{\partial P}{\partial r} + \frac{d}{dr}[(1-\alpha)\sigma_{L,rr}] + \frac{1}{r}[(1-\alpha)(\sigma_{L,rr} - \sigma_{G,\psi\psi})] \tag{2.15}$$

Axial momentum equations for the gas and liquid phases:

$$0 = -\alpha\frac{\partial P}{\partial z} + \frac{1}{r}\frac{d}{dr}[r\alpha(\tau_{G,rz} + \sigma_{G,rz})] - \alpha\rho_G g\cos\theta + P_G \tag{2.16}$$

$$0 = -(1-\alpha)\frac{\partial P}{\partial z} + \frac{1}{r}\frac{d}{dr}[r(1-\alpha)(\tau_{L,rz} + \sigma_{L,rz})] - (1-\alpha)\rho_L g\cos\theta - P_G \tag{2.17}$$

In the above equations r is the radial, z is the axial and ψ is the azimuthal coordinate, whereas $\cos\theta = 1$ for upflow and -1 for downflow. It can be noted that equations (2.14)-(2-17) are similar to those used to study the phase distribution in a bubbly two-phase flow [11,16], although the interpretation of the averaged quantities is different since in these works they are based on the time-averaged two-phase flow model [17]. These difference gives rise to a greater number of turbulent correlations in (2.12) and (2.13) than in the model of [17] which for the present paper is not significant, since these correlations will not be separately modeled (see below). For further discussion on the two-phase flow equations, the reader is referred to Dobran [18].

3. TURBULENCE MODELING AND VOID FRACTION DISTRIBUTION IN THE CORE

The interfacial region between the liquid film and core region of an annular flow is usually covered by a complex system of waves whose structure will be ignored in this paper. Instead, it will be assumed that the core region consists of a time-averaged radius Ri as shown in Fig. 1, and that the liquid is dispersed in the form of droplets. The average interface location corresponds to that of a cylinder of radius Ri.

3.1 Turbulence Model of the Core Region

The turbulent stresses in (2-14)-(2-17) may be modeled: (1) by an assumption that relates the liquid phase turbulence characteristics to the gas phase turbulence characteristics, and (2) by an assumption of the gas phase turbulence.

The behavior of liquid droplets in the turbulent gas depends on the concentration of droplets and on the size of droplets relative to the scale of turbulence. At very low droplet concentrations we can expect that the droplet

interference with other droplets is minimal and may assume that each droplet can be regarded as being alone in the gas. When the droplet concentration is high, they interact directly through collisions and indirectly through the effect of change of the flow field created by the droplets themselves. The size of droplets is also an important variable, since it determines the relaxation time or the characteristic response time of droplets due to the change of their environment. Large droplets in comparison with the scale of turbulence will experience a flow resistance and should follow only large-scale turbulent motions, whereas the small droplets in comparison with the smallest turbulent length scale or Kolmogoroff's micro-scale length will tend to follow all turbulent fluctuations of the gas. Hinze [19] estimated the response time of a particle in a turbulent fluid and concluded that, for the situation when the density of the particle is much larger than that of the fluid, the particle will follow the fluid if its size is an order of magnitude smaller than the Kolmogoroff's micro-scale length. The experiments [20] involving very dilute suspensions of solid particles in air flowing in a vertical pipe indicate that the Kolmogoroff's length scale is about 100μm, whereas an investigation involving a vertical annular-mist flow [21] indicates that the most probable and average droplet diameters are, respectively, 30 and 41μm.

From the above, it may be assumed that the relationship between the liquid phase and gas phase turbulence can be modeled as follows:

$$\sigma_{L,ij} = C_1 q\, \sigma_{G,ij} = Q\sigma_{G,ij} \tag{3.1}$$

where $q=\rho_L/\rho_G$ and C_1 is presumably a constant and of order one. Equation (3.1) can be viewed as representing an equality of liquid phase and gas phase time average of the product of radial and axial velocity fluctuations if $C_1=1$. A value of $C_1<1$ would correspond to the liquid phase turbulent fluctuations of lower amplitude than the gas phase, whereas to the value of $C_1>1$ would correspond the opposite conclusion. Away from the liquid film interface the assumption expressed by (3.1) is reasonable as long as the droplets are sufficiently small and their concentration low (see above), since then they will follow the turbulent fluctuations of the gas phase. Close to the liquid film interface, however, this assumption may break down due to their larger concentration than in the core and because of the presence of multiple scales of turbulence.[3]

To model the gas phase turbulence, a mixing-length model will be employed for the reasons that this model does a credible job in modeling the single-phase turbulent flows and bubbly two-phase flows [11]. Near the tube centerline, however, this model will have to be modified, for otherwise it would predict the unphysical result that the turbulent stress $\sigma_{G,zz}=0$. A simpler model like the eddy-viscosity would predict that $\sigma_{G,rr}=\sigma_{G,\psi\psi}=0$ which is in contradiction with the bubbly flow data [10]. More complicated two-phase flow turbulence modeling is not warranted until simpler models are explored, and due to the very complicated nature of the two-phase flows such modeling may not prove to be very practical.

The turbulent shear stress of the gas phase is, therefore, modeled as

[3] Close to the liquid film interface a number of length scales can be identified, such as the pipe radius, liquid film thickness, time-averaged droplet diameter, and average thickness of the interfacial waves.

follows:

$$\sigma_{G,rz}(r) = \sigma_{G,Ri}(r) + \rho_G \ell_G^2 \left|\frac{dU_G}{dr}\right| \frac{du_G}{dr} \tag{3.2}$$

where

$$\ell_G = k_G(Ri-r) \tag{3.3}$$

is the mixing length and k_G is assumed to be a constant. The shear stress $\sigma_{G,Ri}$ in (3.2) is added for two reasons: (1) to prevent an inconsistency with the assumption (3.1) at the liquid film interface where $\ell_G=0$ and where $\sigma_{G,rz}(Ri)$ may represent the largest contribution to the interfacial shear, and (2) close to the liquid film interface it is expected that the interfacial shear will contribute to the total turbulent energy of the gas phase. Away from the interface, but not close to the centerline of the tube, the effect of the interface should diminish and the mixing length theory should apply. A possible way of constructing an approximation of $\sigma_{G,Ri}$ (which involves an interfacial turbulent length scale) with the above properties is presented in the appendix from where we obtain:

$$\sigma_{G,Ri}(r) = \sigma_{G,Ri}(Ri)\left(\frac{r}{Ri}\right)^2 \tag{3.4}$$

The axial turbulent stress $\sigma_{G,zz}$ will be modeled by the following equation:

$$\sigma_{G,zz} = -\frac{\sigma_{G,rz}}{K_G^2} + \sigma_{G,zzo}(r) \tag{3.5}$$

where K_G^2 is assumed to be constant and where $\sigma_{G,zzo}(r)$ is added to prevent $\sigma_{G,zz}$ from becoming equal to zero at r=0. The value of K_G^2 is expected to be on the order of 0.01 [9].

3.2 Distribution of the Gas Volumetric Fraction in the Core

The equations governing the distribution of the gas volumetric fraction in the core region can be obtained from the momentum equations (2.14)-(2.17) and from the turbulence modeling equations (3.1)-(3.5) with the additional assumptions regarding the nature of characteristic length scales in different regions of the core. By eliminating the pressure gradient between equations (2.14) and (2.15) and using (3.1) results in the following equation for the radial void fraction distribution:

$$-\frac{d\alpha}{dr}\frac{(1-\alpha)+Q\alpha}{\alpha(1-\alpha)(1-Q)} = \frac{1}{\sigma_{G,rr}}\frac{d\sigma_{G,rr}}{dr} + \frac{\sigma_{G,rr}-\sigma_{G,\psi\psi}}{r\,\sigma_{G,rr}} \tag{3.6}$$

which can be integrated to yield:

$$\frac{(1-\alpha)^Q}{\alpha} = C\,\sigma_{G,rr}^{(1-Q)} \exp\left[(1-Q)\int_{Ri}^{r}\frac{\sigma_{G,rr}-\sigma_{G,\psi\psi}}{r'\sigma_{G,rr}}\,dr'\right] \tag{3.7}$$

where C is the constant of integration. Equation (3.7) shows that the void fraction distribution depends on the radial turbulent stress, $\sigma_{G,rr}$, and on the anisotropy of the gas-phase turbulence expressed by the integral. For an isotropic turbulent flow, $\sigma_{G,rr}=\sigma_{G,zz}=\sigma_{G,\psi\psi}$. While no turbulence data appear to exist for an annular flow to judge the degree of anisotropy in the core, it can be noted that bubbly two-phase flow data [9,10] and particle-air data [20] show that the two-phase flow is more isotropic than a single-phase anisotropic flow. By extrapolation it may be assumed, therefore, that a two-phase droplet flow is nearly isotropic. Indeed, by defining

$$f(r) = \frac{\sigma_{G,zz}}{\sigma_{G,rr}} \exp\left[\int_{Ri}^{r} \frac{\sigma_{G,\psi\psi}-\sigma_{G,rr}}{r'\,\sigma_{G,rr}}\,dr'\right] \tag{3.8}$$

the flow isotropy implies that $f(r)=1$. Combining (3.7) and (3.8) gives

$$\sigma_{G,zz} = f(r)\left[\frac{(1-\alpha)^Q}{\alpha C}\right]^{1/(1-Q)} \tag{3.9}$$

The laminar shear stress, $\tau_{G,rz}$, is given by the usual equation

$$\tau_{G,rz} = \mu_G \frac{du_G}{dr} \tag{3.10}$$

and assuming that $du_G/dr<0$, we may eliminate the velocity gradient between (3.2) and (3.10) to obtain:

$$\tau_{G,rz} = -\frac{\mu_G K_G}{\ell_G}\left[\frac{1}{\rho_G}\left(\sigma_{G,zz}-\sigma_{G,zzo}+\frac{\sigma_{G,Ri}}{K_G^2}\right)\right]^{1/2} \tag{3.11}$$

$$\sigma_{G,rz} = -K_G^2\left(\sigma_{G,zz}-\sigma_{G,zzo}\right) \tag{3.12}$$

Adding the axial components of the momentum equation, (2.16) and (2.17), and utilizing (3.1), (3.9), (3.11) and (3.12) gives

$$\frac{1}{r}\frac{d}{dr}\Big[-r(1-\alpha)\tau_{L,rz}+rK_G^2(\alpha+(1-\alpha)Q)\Big(\Big(\frac{(1-\alpha)^Q}{\alpha C}\Big)^{1/(1-Q)} f(r)-\sigma_{G,zzo}\Big) + r\alpha\frac{\mu_G K_G}{\ell_G}\Big[\frac{1}{\rho_G}\Big(\Big(\frac{(1-\alpha)^Q}{\alpha C}\Big)^{1/(1-Q)} f(r)-\sigma_{G,zzo}+\frac{\sigma_{G,Ri}}{K_G^2}\Big)\Big]^{1/2}\Big] + \frac{\partial P}{\partial z} + [\alpha\rho_G+(1-\alpha)\rho_L]g\cos\theta = 0 \tag{3.13}$$

Equation (3.13) is the basic differential equation for the determination of void fraction α in the core region of an annular flow. The distribution of α depends on the turbulence characteristics K_G^2, q, ℓ_G, $f(r)$, $\sigma_{G,zzo}$ and $\sigma_{G,Ri}$, on the liquid and gas fluid properties ρ_L, μ_L, ρ_G and μ_G, on the external flow driving force $\partial P/\partial z$, and on the flow direction. Since detailed experimental data of annular flows are lacking for the determination of these turbulence parameters, in what follows we will utilize the available information from

annular and nonannular flows for the determination of the void fraction by seeking solutions in different regions of the core. The basic approach is to divide the core region into three regions as shown in Fig. 1. In Region I, which is close to the liquid film interface, a steep void fraction gradient exists, whereas in Region II the void fraction is assumed to be constant (as attested by the data [4,5]). In Region III the void fraction profile adjusts itself to the local turbulence characteristics.

3.2.1 Intermediate Core Region - Region II In the intermediate region of the core, between the liquid film interface region and the central region of the tube, the void fraction appears to reach a uniform profile as the data [4-6] show. Adding (2.16) and (2.17) and then integrating from r=0 to r=Ri (where α=0) yields

$$Ri[\tau_{L,rz}(Ri)+\sigma_{L,rz}(Ri)] = -\frac{\partial P}{\partial z}\frac{Ri^2}{2} - \rho_L g\cos\theta\frac{Ri^2}{2} + \rho_L g\cos\theta\left(1-\frac{\rho_G}{\rho_L}\right)\int_0^{Ri}\alpha r\,dr = 0 \tag{3.14}$$

Defining the core-averaged void fraction $\langle\alpha\rangle$ by the equation

$$\langle\alpha\rangle = \frac{1}{\pi Ri^2}\int_0^{Ri}\alpha 2\pi r\,dr \tag{3.15}$$

and using this equation in (3.14) results in an expression for the pressure gradient, i.e.

$$\frac{\partial P}{\partial z} = \frac{2}{Ri}[\tau_{L,rz}(Ri)+\sigma_{L,rz}(Ri)] - \rho_L g\cos\theta\,(1-\langle\alpha\rangle) \tag{3.16}$$

where it is assumed that $\rho_G/\rho_L<<1$. For an air-water mixture at an atmospheric pressure $\rho_G/\rho_L=10^{-3}$ and we may be justified in making this assumption for many two-phase flows.

To determine a uniform distribution of void fraction α_o in Region II, we will invoke the following assumptions:

1. Viscous stresses can be neglected in comparison with the turbulent stresses, pressure gradient, and gravitational force.

2. $Q>>1$.

3. $\left(\frac{(1-\alpha)^Q}{\alpha C}\right)^{1/(1-Q)} = \frac{1}{1-\alpha}\left(\frac{1}{C}\right)^{1/(1-Q)} = \frac{\sigma_{G,rr}(Ri)}{1-\alpha}$

4. $\sigma_{G,zzo}(r)<<\sigma_{G,zz}(r)$

The third assumption above can be justified by using the second assumption and evaluating C in (3.8) and (3.9) at r=Ri. The fourth assumption implies that the contribution of $\sigma_{G,zzo}(r)$ to $\sigma_{G,zz}(r)$ is negligible in Region II. Equation (3.13) is, therefore, reduced to

$$\left[1+\frac{\alpha_o}{(1-\alpha_o)Q}\right]\frac{K_G^2 Q\sigma_{G,rr}(Ri)}{\rho_L g}\frac{1}{r}\frac{d}{dr}(rf(r)) + \frac{1}{\rho_L g}\frac{\partial P}{\partial z} + (1-\alpha_o Bo)\cos\theta = 0 \tag{3.17}$$

where $Bo=1-\rho_G/\rho_L$ is the Buoyancy number. In (3.17) it is clear that we must have

$$\frac{1}{r}\frac{d}{dr}(rf(r)) = \text{constant} \tag{3.18}$$

This condition is somewhat justified for low quality bubbly flows by examining the single-phase anisotropic pipe flow data of Laufer [22]. In the core region of an annular flow, however, no data exist to justify (3.18), but due to the similarity between droplet, bubbly and particulate flows it may be assumed that (3.18) is a valid approximation. From (3.18) it thus follows that

$$\text{constant} = \frac{2f_2}{R_2}\left(1 - \frac{R_1 f_1}{R_2 f_2}\right)/\left(1 - \frac{R_1^2}{R_2^2}\right) \tag{3.19}$$

where $f_1=f(R_1)$ and $f_2=f(R_2)$, and R_1 and R_2 are the boundary radii of Region II as shown in Fig. 1. Substituting (3.18) and (3.19) in (3.17), eliminating the pressure gradient using (3.16) and utilizing the assumption that in Region I $f(r)=f(Ri)=f(R_2)$ and $R_2=Ri$ (see below), we obtain

$$\alpha_o = \langle\alpha\rangle + \frac{2\tau_{L,rz}(Ri)}{\rho_L g Ri\cos\theta} + \frac{2\sigma_{L,rz}(Ri)}{\rho_L g Ri\cos\theta}\frac{R_1}{R_2}\left(\frac{f_1}{f_2} - \frac{R_1}{R_2}\right)/\left(1 - \frac{R_1^2}{R_2^2}\right) \tag{3.20}$$

where use is made of (3.1), (3.5) and (3.8). Since the interfacial shear stress τ_i is defined as

$$\tau_i = -\left[\tau_{L,rz}(Ri)+\sigma_{L,rz}(Ri)\right] \tag{3.21}$$

equation (3.20) is reduced to

$$\alpha_o = \langle\alpha\rangle - \frac{2\tau_i}{\rho_L g Ri\cos\theta} - \frac{2\sigma_{L,rz}(Ri)}{\rho_L g Ri\cos\theta}\left(1 - \frac{f_1 R_1}{f_2 R_2}\right)/\left(1 - \frac{R_1^2}{R_2^2}\right) \tag{3.22}$$

from where it can be observed that for a turbulent liquid film $\alpha_o\approx\langle\alpha\rangle$ for $f_1=\text{order}(f_2)$ and $R_1<<R_2$. For the upflow case $\cos\theta=1$ and $\alpha_o < \langle\alpha\rangle$, whereas for downflow $\cos\theta=-1$ and $\alpha_o > \langle\alpha\rangle$. The assumption that $f_1=\text{order}(f_2)$ may be justified from the single-phase anisotropic pipe flow data [22] and a bubbly two-phase flow analysis [16]. The second assumption of $R_1<<R_2$ can be justified by examining the data of Gill et al. [4].

3.2.2 Interfacial Core Region ~ Region I In region I the void fraction changes from the value of zero at $r=Ri$ to a constant value α_o in Region II, and as the data [4] indicate we will assume that this change occurs in a thin region close to the liquid film interface. Moreover, it will also be assumed that

1. $\sigma_{G,zzo}(r)<<\sigma_{G,zz}(r)$, and $\tau_{L,rz}$ is negligible in comparison with $\sigma_{L,rz}$.
2. $Q>>1$.
3. $\left(\frac{(1-\alpha)}{\alpha C}^Q\right)^{1/(1-Q)} = \frac{\sigma_{G,rr}(Ri)}{1-\alpha}$.

4. $f(r)=f(Ri)$ and $r=Ri$, giving $\frac{1}{r}\frac{d}{dr}(rf(r))=\frac{f(Ri)}{Ri}$.
5. Validity of (3.4).
6. Balance between the void fraction gradient, $d\alpha/dr$, and the terms in (3.13) involving pressure gradient and gravity (as may be justified a posteriori).

With the above assumptions, it follows that the scaling of the radial coordinate according to

$$\xi = \frac{Ri - r}{\Delta} \tag{3.23}$$

in (3.13) yields:

$$\Delta^2 = \frac{\mu_G K_G}{2k_G\rho_L g}\left[\frac{f(Ri)\sigma_{G,rr}(Ri)}{\rho_G}\right]^{1/2} \tag{3.24}$$

and

$$\frac{K_G^2 Q\sigma_{G,rr}(Ri)f(Ri)}{\rho_L g Ri}\left[1 + \frac{\alpha}{Q(1-\alpha)} - \frac{Ri}{Q(1-\alpha)^2\Delta}\frac{d\alpha}{d\xi}\right] + \frac{\Delta}{Ri}\left[\frac{2}{\xi}(1-\alpha)^{-1/2}\alpha^{3/2}\right.$$
$$\left. - \frac{2}{\xi}(1-\alpha)^{1/2}\alpha^{1/2}\right] - \frac{2}{\xi}\alpha^{1/2}(1-\alpha)^{-1/2}\frac{d\alpha}{d\xi} + \frac{2}{\xi^2}\alpha^{3/2}(1-\alpha)^{-1/2}$$
$$- \frac{1}{\xi}\alpha^{1/2}(1-\alpha)^{-3/2}\frac{d\alpha}{d\xi} + \frac{\partial P}{\partial z}\frac{1}{\rho_L g} + (1-\alpha Bo)\cos\theta = 0 \tag{3.25}$$

By defining the parameters

$$\eta = \frac{1}{2}k_G^2 N_L^2\left(\frac{\mu_L}{\mu_G}\right)^2\left(\frac{\rho_G}{\rho_L}\right) = \frac{1}{2}k_G^2 N_G^2 \tag{3.26}$$

$$N_L^2 = \frac{D^3 g\rho_L(\rho_L-\rho_G)Bo}{\mu_L^2}, \qquad N_G^2 = N_L^2(1-Bo)\left(\frac{\mu_L}{\mu_G}\right)^2 \tag{3.27}$$

where N_L is the two-phase Grashof number representing the ratio of buoyancy to viscous forces, whereas the parameter η represents the combined effect of turbulence intensity, buoyancy and viscous forces. Eliminating in (3.25) the pressure gradient by using (3.17) gives a differential equation for α, i.e.

$$\frac{d\alpha}{d\xi} = \frac{\left(\frac{\Delta}{Ri}\right)^4\eta\left[\alpha(1-\alpha)^{-1} - \alpha_o(1-\alpha_o)^{-1}\right] + \frac{2}{\xi^2}\alpha^{3/2}(1-\alpha)^{-1/2} - Bo(\alpha-\alpha_o)\cos\theta}{\left(\frac{\Delta}{Ri}\right)^3\eta(1-\alpha)^{-2} + \frac{1}{\xi}\alpha^{1/2}(1-\alpha)^{-3/2}(3-2\alpha)} \tag{3.28}$$

where we assumed that: (1) the term in square brackets in (2.25) when multiplied by Δ/Ri is much smaller than the remaining terms, and (2) the film thickness is small compared to the tube radius. For an air-water mixture at atmospheric pressure $\mu_G=2\times10^{-5}$ Kg/m-s, $\rho_L=10^3$ Kg/m^3, $g=10$ m/s^2 and $\rho_G=1$ Kg/m^3, assuming that $K_G=1$, and using for $Ri=2\times10^{-2}$ m and for $K_G^2 f(Ri)\sigma_{G,rr}(Ri)q=\tau_i$ a value of 10^2 N/m^2 (see [23,24], for example, for typical values), we find that $\Delta/Ri=10^{-3}$ and may be justified in our assumptions. The solution of (3.28) is discussed in the next section where for upflow the void fraction may possess a peak in Region I, whereas for downflow no such peak is predicted.

3.2.2 Central Core Region - Region III In Region III it is reasonable to assume the following:

1. Viscous stresses are much smaller than the turbulent stresses.

2. $\alpha+(1-\alpha)Q=(1-\alpha)Q$ or $Q\gg\frac{\alpha}{1-\alpha}$.

3. $\left(\frac{(1-\alpha)}{\alpha C}^{Q}\right)^{1/(1-Q)}=\frac{1}{1-\alpha}\sigma_{G,rr}(Ri)$ as in Regions I and II.

4. $\sigma_{G,zzo}(r)=\sigma_{G,zzo}(0)$, i.e., a constant term in the Taylor series expansion of $\sigma_{G,zzo}(r)$ about $r=0$.

5. $f(r)=\text{constant}=f(0)$.

6. Balance in (3.13) between the void fraction gradient and terms involving the axial pressure gradient and gravity.

Using assumptions 3 and 5 and equation (3.9) gives

$$\frac{\sigma_{G,zz}(r)}{\sigma_{G,zz}(0)}=\frac{f(r)}{1-\alpha}\,\frac{1-\alpha(0)}{f(0)}=\frac{1-\alpha(0)}{1-\alpha} \tag{3.29}$$

and from (3.5) we obtain

$$\sigma_{G,zz}(0)=\sigma_{G,zzo}(0) \tag{3.30}$$

Utilizing assumptions 1, 2 and 3, (3.13) is reduced to

$$\frac{1}{r}\frac{d}{dr}\left[r\,K_G^2(1-\alpha)Q\left(\frac{\sigma_{G,rr}(Ri)f(r)}{1-\alpha}-\sigma_{G,zzo}(r)\right)\right]+\frac{\partial P}{\partial z}+(1-\alpha)\rho_L g\cos\theta=0 \tag{3.31}$$

Furthermore, from (3.9), (3.29), (3.30) and assumption 4 it follows that

$$\sigma_{G,rr}(Ri)f(r)=(1-\alpha)\sigma_{G,zz}(r)=[1-\alpha(0)]\sigma_{G,zz}(0)=[1-\alpha(0)]\sigma_{G,zzo}(0) \tag{3.32}$$

which upon the substitution into (3.31) and elimination of pressure gradient by means of (3.17)-(3.19) with $f_2=f(Ri)$ and $R_2=Ri$, gives

$$\frac{1}{r}\frac{d}{dr}\left\{r[1-\alpha(0)-(1-\alpha)]\right\}-\frac{\sigma_{G,zz}(Ri)}{\sigma_{G,zz}(0)}\,\frac{2}{Ri}\,\frac{(1-R_1f_1/R_2f_2)}{(1-R_1^2/R_2^2)}+\frac{\rho_L g\cos\theta}{K_G^2Q\sigma_{G,zz}(0)}[1-\alpha-(1-\alpha_o)]=0 \tag{3.33}$$

Defining a scaling of the radial coordinate according to

$$Y=\frac{r}{\delta} \tag{3.34}$$

and using assumption 6 in this equation gives:

$$\delta=\frac{K_G^2Q\sigma_{G,zz}(0)}{\rho_L g} \tag{3.35}$$

$$\frac{1}{Y}\frac{d}{dY}\left\{Y[1-\alpha(0)-(1-\alpha)]\right\}-\frac{\sigma_{G,zz}(Ri)}{\sigma_{G,zz}(0)}\,\frac{2\delta}{Ri}\,\frac{(1-R_1f_1/R_2f_2)}{(1-R_1^2/R_2^2)}+[1-\alpha-(1-\alpha_o)]\cos\theta=0 \tag{3.36}$$

Since Region III can be defined as a region with $\delta/Ri\ll1$, we can obtain from (3.36) the void fraction distribution equation, i.e.

$$\frac{d}{dY}Y(1-\alpha)-Y(1-\alpha)\cos\theta=1-\alpha(0)-Y(1-\alpha_o)\cos\theta \tag{3.37}$$

from where an integration yields

$$\alpha=\alpha_o-\frac{1}{Y}C_2\exp[Y\cos\theta]-\frac{\alpha(0)-\alpha_o}{Y\cos\theta} \tag{3.38}$$

with C_2 being the constant of integration. For upflow $\cos\theta=1$ and since it is required that limit $\alpha=\alpha_o$, as $Y\to\infty$, this gives $C_2=0$. As $Y\to0$ at fixed δ, it is also required that $\alpha(0)=\alpha_o$ for α to be bounded, giving thus

$$\alpha(Y)=\alpha_o \quad \text{for } \underline{\text{upflow}} \tag{3.39}$$

For downflow $\cos\theta=-1$ and limit $\alpha=\alpha_o$, as $Y\to\infty$, is satisfied without restricting C_2. However, as $Y\to0$ it follows that $C_2=\alpha(0)-\alpha_o$, and therefore

$$\alpha(Y)=\alpha_o+\frac{\alpha(0)-\alpha_o}{Y}(1-e^{-Y}) \quad \text{for } \underline{\text{downflow}} \tag{3.40}$$

The interesting properties of the void fraction distribution equation for downflow are the gas coring effect and apparent arbitrariness of $\alpha(0)$. This is discussed further in the following section.

In summary, the void fraction distribution in the core region of an

annular flow is expressed by (3.28) in Region I, by (3.22) in Region II, and by (3.38) in Region III, with the properties of these equations discussed in the following section.

4. DISCUSSION OF THE VOID FRACTION PROFILES

4.1 Vertical Upflow - cosθ=1

The void fraction distribution in upflow determined from (3.22), (3.28) and (3.38 is qualitatively illustrated in Fig. 2. The dot-dashed curve in this figure represents the solution of the equation

$$\left(\frac{\Delta}{Ri}\right)^4 \eta\left[\alpha(1-\alpha)^{-1}-\alpha_o(1-\alpha_o)^{-1}\right] + \frac{2}{\xi^2}\alpha^{3/2}(1-\alpha)^{-1/2}-Bo(\alpha-\alpha_o) = 0 \qquad (4.1)$$

which is obtained by setting $d\alpha/d\xi=0$ in (3.28). In finding the physical solution for the void fraction distribution with fixed values of the parameters Δ/Ri, η, Bo and α_o, it is first noted that (3.28) has an infinite number of solutions which pass through the singular point at $\alpha=0$ and $r=Ri$ (five such solutions are sketched in the figure). Since the void fraction determined from (3.28) and (3.39) must be compatible with the Region II solution, it is evident that there is only one physical solution which satisfies (3.22), (3.28) and (3.39), simultaneously. For a turbulent liquid film, equation (3.22) gives $\alpha_o=\langle\alpha\rangle$, and since for a high quality flow $\langle\alpha\rangle=0.95$-1, the analysis predicts a very steep gradient of α in Region I or in the region close to the liquid film interface.

The upward annular flow data of Gill et al. [4] give $\alpha_o=0.998$ and, indeed, show a very steep void fraction gradient close to the liquid film, but unfortunately their measurements were unable to resolve this gradient in sufficient detail to warrant a detailed comparison with the present analysis. The presence of a physical peak in the void fraction profile close to the liquid film cannot be deduced from these data nor it is being necessarily predicted by the analysis at high average void fractions as iluustrated in Figs. 3 and 4. The data [12] pertaining to an upward flow of a dense phase which is dispersed in a lighter continuous phase in a vertical tube show that the lighter phase tends to concentrate close to the tube wall and, therefore, may be used as a justification of the present theoretical prediction of the void fraction peak close to the liquid film interface. It should be noted, however, that these data pertain to laminar flow and that their use in validating the present prediction may not be completely appropriate.

The void fraction distribution as a function of the normalized radial coordinate, r/Ri, determined from (3.22), (3.28) and (3.39), depends on the parameters Δ/Ri, η, Bo and $\langle\alpha\rangle$, and it is is shown in Figs. 3 and 4. In Fig. 3 $\Delta/Ri=10^{-3}$, whereas in Fig. 4 $\eta=10^8$, with the results being generated with $\alpha_o=\langle\alpha\rangle$ and Bo=0.999.

The effect of increasing the parameter η at constant $\langle\alpha\rangle$, Bo and Δ/Ri is: (1) to decrease the gas phase concentration close to the liquid film interface at low $\langle\alpha\rangle$ only, and (2) to flatten the void fraction profile in the core as may be seen in Fig. 3. The variation of the parameter Δ/Ri (or interfacial shear stress as may be seen from (3.34)), at constant $\langle\alpha\rangle$ and η, is illustrated in Fig. 4 from where it may be concluded that an increase in the shear stress

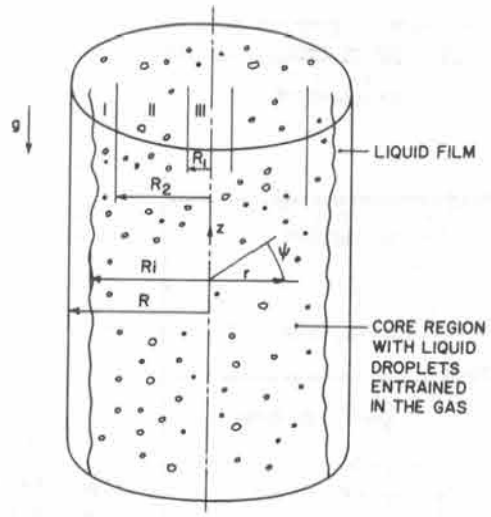

Fig. 1 Annular two-phase flow in a tube.

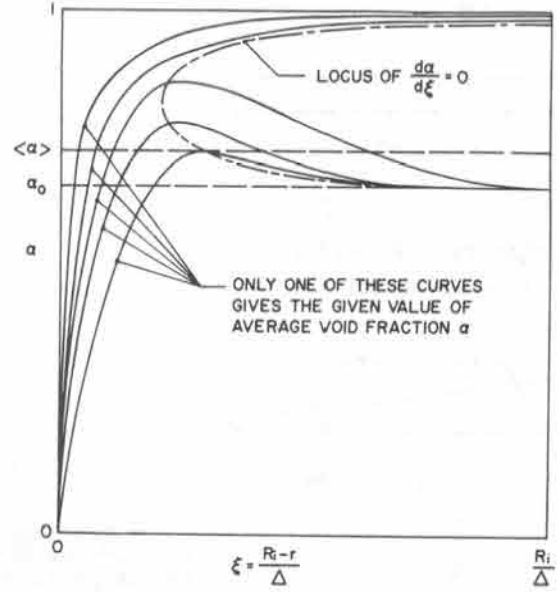

Fig. 2 Qualitative solution properties of the void fraction distribution in upflow for fixed Δ/Ri, η and Bo.

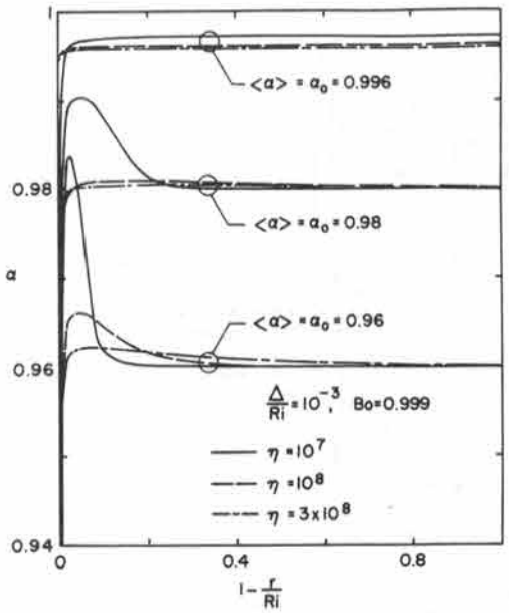

Fig. 3 Radial void fraction distributions in upflow as a function of $\langle\alpha\rangle$ and η for $\Delta/Ri=10^{-3}$.

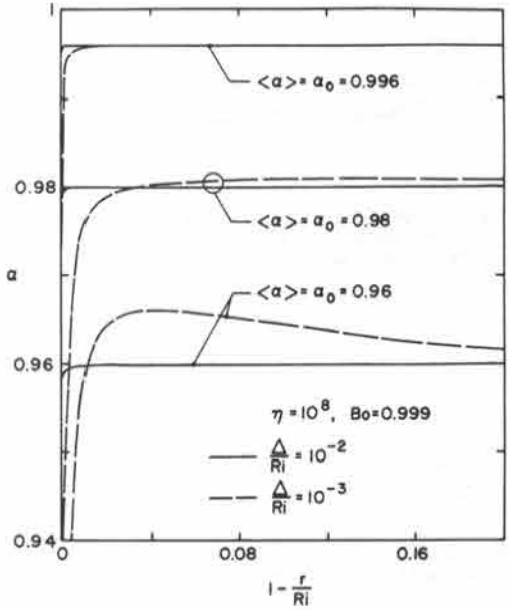

Fig. 4 Radial void fraction distributions in upflow as a function of $\langle\alpha\rangle$ and Δ/Ri for $\eta=10^{8}$.

at the liquid film interface produces flatter void fraction profiles. Higher values of the average gas phase concentrations, $\langle\alpha\rangle$, have the effect of producing a more uniform void fraction distribution in the core, and at very high values of $\langle\alpha\rangle$ no void fraction peak is predicted close to the film interface. As noted above, these results are also consistent with data [4,8]. The variation of the buoyancy number Bo has a negligible effect on the void fraction distribution at high values of this parameter for which the model applies.

4.2 Vertical Downflow - $\cos\theta=-1$

For the vertical downflow, equation (3.28) does not predict a peak in the void fraction profile close to the liquid film interface; instead, the prediction of a peak or coring effect comes from the Region III solution or equation (3.38) (or (3.40)). As noted earlier, $\alpha(0)$ in (3.40) is arbitrary, with (3.28) having only one solution and implying that it must be chosen in such a way that the solution expressed by (3.22) is also satisfied. This is qualitatively shown in Fig. 5.

The void fraction distributions in the core are depicted in Figs. 6 and 7 to illustrate the effect of parameters $\langle\alpha\rangle$, Δ/Ri and η. In generating the results in these figures the void fraction distribution in Region III is assumed to correspond to α_o as in Region II, and α_o is determined such that the profile produces the given value of $\langle\alpha\rangle$, in order to eliminate the modeling difficulties with additional variables $\alpha(0)$ and $\sigma_{G,zz}(0)$. The buoyancy number is taken as Bo=0.999. Contrary to some situations of the vertical upflow, the effect of increasing the parameter η at constant $\langle\alpha\rangle$ and Δ/Ri is to increase the gas phase concentration close to the liquid film interface and to flatten the void fraction profile in the core as depicted in Fig. 6. At constant $\langle\alpha\rangle$ and η, however, larger values of Δ/Ri (or larger interfacial shear stresses) produce more uniform void fraction profiles in the core as in the upflow situation. These results are also consistent with the downflow data [8], and the buoyancy number has a negligible effect on the void fraction distribution.

The void fraction peak at the pipe centerline or the coring effect is shown qualitatively in Fig. 5 and can be quantitatively determined by selecting the curve which produces a given $\langle\alpha\rangle$. Although no data exist to substantiate the coring effect in annular flow, this effect is real for flows without the liquid film and it has been shown to occur by the lighter phase. In bubbly flows this is confirmed by the data of [7,8], whereas in flows where the dispersed phase is denser than the continuous phase it is confirmed by the data of [12].

5. DISTRIBUTION OF LIQUID AND GAS FLOW PROPERTIES

The void fraction distribution equation expressed by (3.28) will be used in this section to study the distribution of liquid and gas flow properties in an annular dispersed flow. The void fraction in the intermediate and central core regions will be assumed to be equal to α_o=constant, for both upflow and downflow situations. The interfacial shear stress τ_i can be obtained from (3.21) by using (3.1) and by assuming that the liquid viscous shear stress is negligible in comparison with the turbulent stress at the liquid film interface, i.e.

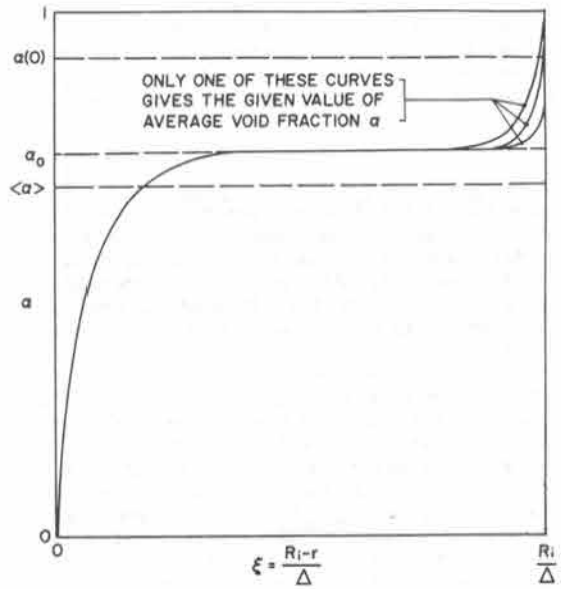

Fig. 5 Qualitative solution properties of void fraction distribution in downflow for fixed Δ/Ri, η and Bo.

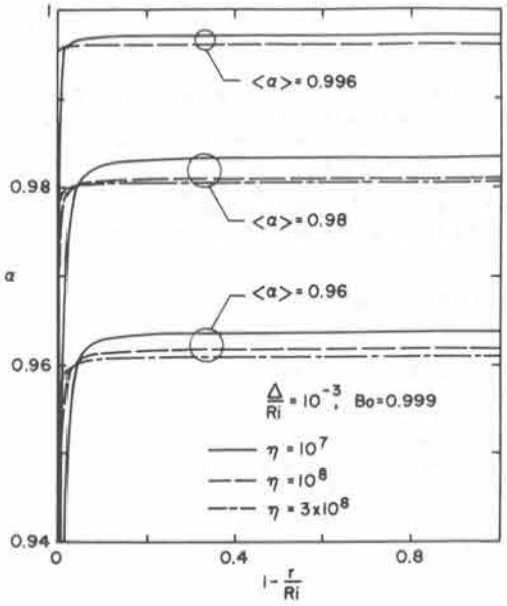

Fig. 6 Radial void fraction distributions in downflow as a function of <α> and η for $\Delta/Ri=10^{-3}$.

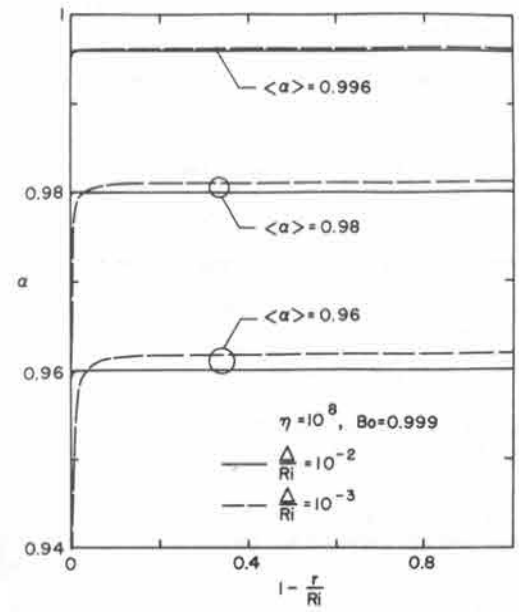

Fig. 7 Radial void fraction distributions in downflow as a function of <α> and Δ/Ri for $\eta=10^8$.

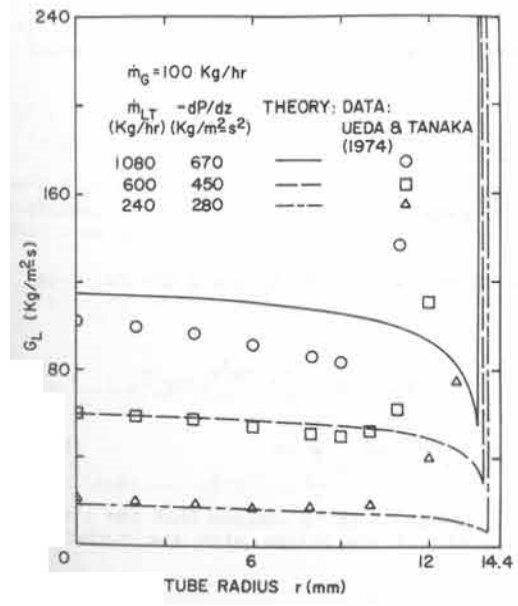

Fig. 8 Comparison of predicted liquid droplets mass fluxes in downflow with air-water data at 0.1MPa.

$$\tau_i = -[\sigma_{L,rz}(Ri)+\tau_{L,rz}(Ri)] \approx -\sigma_{L,rz}(Ri) = -C_1 q \sigma_{G,rz}(Ri) \qquad (5.1)$$

5.1 Gas and Liquid Velocity Distributions in the Core

Adding the axial components of the momentum equation (2.16) and (2.17) results in the following expression:

$$0 = -\frac{\partial P}{\partial z} + \frac{1}{r}\frac{d}{dr}[r\alpha(\tau_{G,rz}+\sigma_{G,rz})+r(1-\alpha)(\tau_{L,rz}+\sigma_{L,rz})] - [\alpha\rho_G+(1-\alpha)\rho_L]\cos\theta \qquad (5.2)$$

and an integration of this equation from $r=0$ to $r>Ri$ and noting that $\alpha(r\geq Ri)=0$ results in

$$0 = -\frac{\partial P}{\partial z}\frac{r^2}{2} + r(\tau_{L,rz}+\sigma_{L,rz}) - g\cos\theta \int_0^{r>Ri} [\alpha\rho_G+(1-\alpha)\rho_L]r\, dr \qquad (5.3)$$

where $\partial P/\partial z$ is an r-direction average axial pressure gradient. Denoting by τ_L the total shear stress in the liquid film, i.e.

$$\tau_L = -(\sigma_{L,rz}+\tau_{L,rz}) \qquad (5.4)$$

and using the definition of the core average void fraction equation (3.15), equation (5.3) is reduced to

$$\tau_L = -(\frac{\partial P}{\partial z} + \rho_L g\cos\theta)\frac{r}{2} + (\rho_L-\rho_G)\langle\alpha\rangle\frac{Ri^2}{2r}g\cos\theta \qquad (5.5)$$

from which we may obtain the wall shear stress, $\tau_w=\tau_L(r=R)$, and the interfacial shear stress, $\tau_i=\tau_L(r=Ri)$. Hence:

$$\tau_w = -(\frac{\partial P}{\partial z} + \rho_L g\cos\theta)\frac{R}{2} + (\rho_L-\rho_G)\langle\alpha\rangle\frac{Ri^2}{2R}g\cos\theta \qquad (5.6)$$

$$\tau_i = -(\frac{\partial P}{\partial z} + \rho_L g\cos\theta)\frac{Ri}{2} + (\rho_L-\rho_G)\langle\alpha\rangle\frac{Ri}{2}g\cos\theta \qquad (5.7)$$

Equation (5.2) may also be integrated from $r>0$ to $r=Ri$ to yield the following result:

$$0 = -\frac{\partial P}{\partial z}\frac{1}{2}(Ri^2-r^2) + Ri\,\sigma_{L,rz}(Ri) - r\alpha(\tau_{G,rz}+\sigma_{G,rz}) - r(1-\alpha)\sigma_{L,rz} - \rho_L\frac{1}{2}(Ri^2-r^2)g\cos\theta + (\rho_L-\rho_G)g\cos\theta\int_r^{Ri}\alpha r\, dr \qquad (5.8)$$

where (consistent with an assumption in section 3 it is assumed that the liquid viscous stress in the core is negligible in comparison with the turbulent

stress. Eliminating $\sigma_{G,rz}(Ri)=\sigma_{G,Ri}(Ri)$ in (3.4) by means of (5.1) and substituting for $\sigma_{G,Ri}(r)$ in (3.2), and physically requiring that $du_G/dr<0$, it follows that the turbulent gas shear stress may be written as:

$$\sigma_{G,rz}(r) = -\frac{\tau_i}{C_1 q}(\frac{r}{Ri})^2 - \rho_G k_G^2(Ri-r)^2(\frac{du_G}{dr})^2 \qquad (5.9)$$

Substituting this equation into (3.1), the liquid phase turbulent shear stress becomes:

$$\sigma_{L,rz}(r) = -\tau_i(\frac{r}{Ri})^2 - C_1 q\rho_G k_G^2(Ri-r)^2(\frac{du_G}{dr})^2 \qquad (5.10)$$

Substituting (3.10), (5.9) and (5.10) into (5.8) and rearranging the equation results in the governing equation for the gas velocity profile in the core region:

$$\rho_G k_G^2(Ri-r)^2 r[\alpha+C_1 q(1-\alpha)](\frac{du_G}{dr})^2 - r\alpha\mu_G(\frac{du_G}{dr}) + \frac{\tau_i}{C_1 q}(\frac{r}{Ri})^2 r[\alpha+C_1 q(1-\alpha)] - \frac{\partial P}{\partial z}\frac{1}{2}(Ri^2-r^2) - Ri\tau_i - \frac{1}{2}(Ri^2-r^2)\rho_L g\cos\theta + (\rho_L-\rho_G)g\cos\theta\int_r^{Ri}\alpha r\, dr = 0 \qquad (5.11)$$

Before proceeding with the solution of (5.11) it is convenient to transform it into a nondimensional form. Towards this objective the following variables frequently used in single-phase turbulent flow are introduced:

$$r=R-Y\,, \qquad \delta = R - Ri \qquad (5.12)$$

$$u_G^+ = \frac{u_G}{u^*}\,, \qquad u^* = (\frac{\tau_w}{\rho_L})^{1/2} \qquad (5.13)$$

$$Y^+ = \frac{u^* Y\rho_L}{\mu_L}\,, \qquad \delta^+ = \frac{u^*\delta\rho_L}{\mu_L}\,, \qquad R^+ = \frac{u^* R\rho_L}{\mu_L} \qquad (5.14)$$

where Y is the distance from the tube wall and δ is the continuous liquid layer thickness. Eliminating the pressure gradient, $\partial P/\partial z$, by means of (5.7) and after some algebra and using (5.6) it can be shown that (5.11) reduces to

$$(1-Bo)k_G^2(Y^+-\delta^+)^2(1-\frac{Y^+}{R^+})[\frac{C_1}{1-Bo}+(1-\frac{C_1}{1-Bo})\alpha](\frac{du_G^+}{dY^+})^2 + \frac{\mu_G}{\mu_L}\alpha(1-\frac{Y^+}{R^+})\frac{du_G^+}{dY^+} + [1-\frac{\delta^+}{R^+}+\frac{1}{16}N_L^2\langle\alpha\rangle\cos\theta\frac{1}{(R^+)^3}(1-\frac{\delta^+}{R^+})(2-\frac{\delta^+}{R^+})\delta^+]\frac{(1-Y^+/R^+)^2}{(1-\delta^+/R^+)}[\frac{(1-Y^+/R^+)}{(1-\delta^+/R^+)}[1-(1-\frac{1-Bo}{C_1})\alpha]-1] - \frac{1}{16}N_L^2\cos\theta\frac{1}{(R^+)^2}[\langle\alpha\rangle[(1-\frac{\delta^+}{R^+})^2-(1-\frac{Y^+}{R^+})^2] - \frac{2}{R^+}\int_{\delta^+}^{Y^+}\alpha(1-\frac{Y^+}{R^+})dY^+] = 0 \qquad (5.15)$$

This equation may also be written in the condensed form as follows:

$$A_1\left(\frac{du_G^+}{dY^+}\right)^2 + A_2\left(\frac{du_G^+}{dY^+}\right) + A_3 = 0 \qquad (5.16)$$

where the definition of A_1, A_2 and A_3 is clear by a reference to (5.15). Physically we expect that $du_G^+/dY^+ \geq 0$, and since $A_1 \geq 0$ and $A_2 \geq 0$, (5.16) can be expressed as

$$\frac{du_G^+}{dY^+} = -\frac{1}{2}\frac{A_2}{A_1} + \frac{1}{2}\left[\left(\frac{A_2}{A_1}\right)^2 - 4\left(\frac{A_3}{A_1}\right)\right]^{1/2} \qquad (5.17)$$

which may be solved numerically. In (5.15) or (5.17) the void fraction α is determined from (3.28) and by assuming that $\alpha(r) = \alpha_c = \text{constant}$ in the intermediate and central core regions. At the tube centerline ($Y^+ = R^+$) it may be shown that $A_1 = A_2 = A_3 = 0$ and that in the limit as $Y^+ \to R^+$: $A_2/A_1 = \text{finite}$, $A_3/A_1 = 0$ and $du_G/dY = 0$.

From (5.17) and given tube geometry and gas-liquid properties, the solution of the nondimensional gas velocity depends on the continuous liquid film thickness δ^+, turbulence properties C_1 and k_G, void fraction distribution α, and on the flow direction or $\cos\theta$. The liquid droplet velocity distribution in the core of an annular flow can be determined from the knowledge of a drag law which enters into the momentum interaction term p_G in (2.16) and (2.17). Because at the present no reliable estimates of p_G in the radial direction exist, and consistent with the turbulence modeling equation (3.1), it will be assumed henceforth that in the core the mean liquid and gas velocities are the same, i.e.

$$u_L^+ = u_G^+ = u_L^+(\delta^+,\ C_1,\ k_G,\ \alpha,\ \langle\alpha\rangle,\ \cos\theta,\ \text{fluid properties, tube geometry}) \qquad (5.18)$$

5.2 Velocity Distribution in the Continuous Liquid Layer Region

The velocity distribution in the liquid film will be modeled by the universal velocity profile of single-phase pipe flow, principally because of its simplicity and to a lesser degree because it gives credible results for the global hydrodynamic flow parameters [2]. Hence

$$1.\quad u^+ = Y^+ \ ; \quad W_f^+ = \frac{1}{2}(\delta^+)^2 \ ; \quad Y^+ \leq \delta^+ \leq 5 \qquad (5.19)$$

$$2.\quad u^+ = Y^+ \ ; \quad Y^+ \leq 5$$

$$u^+ = -3.05 + 5\,\ell n Y^+ \ ; \quad 5 < Y^+ \leq \delta^+ \leq 30 \qquad (5.20)$$

$$W_f^+ = 5\delta^+\,\ell n\delta^+ - 8.05\delta^+ + 12.51$$

$$3.\quad u^+ = Y^+ \ ; \quad Y^+ \leq 5$$

$$u^+ = -3.05 + 5\,\ell n Y^+ \ ; \quad 5 < Y^+ \leq 30 \qquad (5.21)$$

$$u^+ = 5.5 + 2.5\,\ell n Y^+ \ ; \quad 30 < Y^+ \leq \delta^+$$

$$W_f^+ = 2.5\delta^+\,\ell n\delta^+ + 3\delta^+ - 64$$

where

$$W_f^+ = \int_0^{\delta^+} u^+\, dY^+ \qquad (5.22)$$

is the nondimensional liquid film flow-rate.

5.3 Liquid and Gas Flow-Rates

The liquid film mass flow-rate, m_f, and the liquid droplet mass flow-rate in the core, m_e, are defined as follows:

$$m_f = 2\pi R\rho_L \int_0^{\delta} Y u_L\, dY = 2\pi R\mu_L W_f^+ \qquad (5.23)$$

$$m_e = \int_0^{Ri} \rho_L(1-\alpha)u_L 2\pi r\, dr = 2\pi R\mu_L \int_0^{Ri^+}(1-\alpha)u_L^+ \frac{r^+}{R^+}\, dr^+ \qquad (5.24)$$

whereas the total liquid flow-rate is given by

$$m_{LT} = m_f + m_e = 2\pi R\mu_L\left[W_f^+ + \int_0^{Ri^+}(1-\alpha)u_L^+\frac{r^+}{R^+}\, dr^+\right] \qquad (5.25)$$

The gas flow-rate, m_G, is found from

$$m_G = \int_0^{Ri} \rho_G \alpha u_G 2\pi r\, dr = (1-Bo)2\pi R\mu_L \int_0^{Ri^+}\alpha u_G^+ \frac{r^+}{R^+}\, dr^+ \qquad (5.26)$$

and the liquid droplets entrainment ratio, e, is defined as follows:

$$e = \frac{m_e}{m_{LT}} \qquad (5.27)$$

An additional parameter that is useful for comparing the results with data is the liquid droplets mass flux, defined by

$$G_L = \rho_L u^*(1-\alpha)u_L^+ \qquad (5.28)$$

5.4 Independent Parameters and Solution Procedure

The most common independent parameters in annular flow experiments are comprised of the liquid and gas mass flow-rates, m_{LT} and m_G, pressure gradient, $\partial P/\partial z$, tube geometry or pipe diameter D, and specification of upflow or

downflow. With these considerations in view, the following solution procedure for the annular flow properties was adopted:

1. The fluid properties (ρ_L, ρ_G, μ_L, μ_G), tube diameter (D=2R), flow direction ($\cos\theta$), turbulence coefficients (k_G, C_1), and flow parameters (m_{LT}, m_G, $\partial P/\partial z$) are assumed known.

2. Assume the film thickness δ.

3. Assume the entrainment ratio e.

4. From (5.27), (5.25) and (5.23) obtain m_e, m_f and W_f^+.

5. Obtain δ^+ from (5.19), (5.20) or (5.21).

6. Determine u^* and τ_w from (5.14) and (5.13).

7. Obtain the average void fraction from (5.6).

8. Solve for the interfacial shear stress from (5.7).

9. Determine Δ from (3.24), since $\Delta^2=\frac{\mu_G}{2k_G\rho_L g}\left(\frac{\tau_i}{C_1\rho_L}\right)^{1/2}$

10. Solve for the void fraction distribution from (3.28).

11. Obtain gas and liquid velocities from (5.17) and (5.18).

12. Determine m_G from (5.26) and m_{LT} from (5.25) and compare with given values in step 1.

13. If the predicted m_G matches the given value move to the next step, otherwise assume a new value of e in step 3 and repeat calculations.

14. If the predicted m_{LT} matches the given value the solution has been completed, otherwise vary δ in step 2 and repeat calculations.

15. Compute all other variables of interest, including the mean film thickness δ_m defined by

$$\delta_m = Y\big|_{\alpha=0.5} \qquad (5.29)$$

16. Study the effects of turbulence parameters, tube geometry, fluid properties, and flow orientation by repeating calculations from step 1.

The mean film thickness definition (5.29) is consistent with the thickness measured by a conductance probe when the probe is in contact with the gas phase one half of the total time.

6. RESULTS AND DISCUSSION

In this section the model predictions will be compared with the experimental data of air-water upflow and downflow in different diameter tubes. Utilizing the experimental values of the pressure gradient and gas and total liquid flow-rates, Table 1 shows a comparison between the predicted wall shear stress, continuous liquid film thickness, mean film thickness, liquid film crest thickness, and liquid entrainment ratio with the data of Ueda et al. [23,24] and Gill et al. [4,5]. The data in the table correspond to 0.1 MPa in a 28.8 mm diameter tube [23,24], and 0.15 MPa in a 31.8 mm diameter tube [4,5]. The entrainment ratio e_{18} signifies the fraction of the total liquid flow in the tube through the core of the tube with a diameter of 18.8 mm which is used for the purpose of comparing the model's prediction with the data of [23,24]. The results were generated with k_G=0.65 for the data of [23,24], with k_G=0.6 for the data of [5], and with k_G=0.45 for the data of [4]. In all calculations it was assumed that C_1=1. These values of turbulence constants were found to produce the best comparison of theory with data of local droplet mass fluxes.

As shown in Table 1, the predicted wall shear stress, mean film thickness and entrainment ratio e_{18} are in good accord with the experiment, with the wall shear stress and mean film thickness being in error by about 20%. The predicted and measured entrainment ratios agree within ±6% of each other. The predicted values of continuous liquid film thickness and film crest thickness are not very good which may be attributed to the poor prediction of the void fraction distribution close to the liquid film interface as a result of the explicit neglect of the interfacial waves in the model.

The liquid droplets mass flux computed from (5.28) is compared with the downflow data [23] in Fig. 8, and with the upflow data [24] in Fig. 9, for a fixed value of the gas mass flow-rate of 100 Kg/hr. Except close to the liquid film interface where the validity of data is also doubtful, the comparison between the predition and experiment is very reasonable. The model predicts a local minimum close to the liquid film interface for all cases in Figs. 8 and 9 and this trend is in good accord with the data even at lower liquid mass fluxes where the experimental trend does not appear to be clearly discernable due to the flattening of the liquid mass flux curves.

Figures 10 and 11 illustrate the velocity and void fraction profiles for the situations in Figs. 8 and 9, respectively. Here, the comparison with the data is not possible, but the predicted trends agree well with the upflow data of Gill et al. [5]. The velocity decreases near the tube centerline and increases near the film interface as the total liquid flow decreases at a fixed gas flow-rate, for both upflow and downflow situations. Figures 10 and 11 also show that as the total liquid flow decreases at a fixed gas flow, the core void fraction increases and liquid film thickness decreases which is in accord with the upflow data of Gill [5]. It should be noted that here there are no peaks of the void fraction close to the film interface because of the high core-averaged void fraction and high values of Δ/Ri as discussed in section 3. As the liquid flow-rate is increased in Figs. 10 and 11 the velocity profiles seem to approach more the parabolic profiles, in conformity with data [5].

Figure 12 shows a comparison of the predicted results of the liquid droplets mass fluxes with the upflow data of Gill et al. [5] at a fixed gas mass flow-rate of 136 Kg/hr, whereas Fig. 13 depicts the predicted velocity and void fraction profiles for the three different liquid flow-rates in Fig. 12. The results in these figures were generated with the turbulence constants k_G=0.6 and C_1=1. Although the predicted void fraction profile in the core compares well with the experiments in Fig. 13 for the situation of m_{LT}=227 Kg/hr, the predicted core velocity profile is flatter and its centerline value underpredicted by about 25%.

Table 1. Comparison of the predicted flow parameters with the experimental data

$\dot{m}_{LT}$ Kg/hr	$\dot{m}_G$ Kg/hr	$-\frac{dP}{dz}$ Kg/m^2s^2	τ_w $Kg/m\text{-}s^2$ Theo. Exp.	$\delta \times 10^3$ (m) Theo. Exp.	$\delta_m \times 10^3$ (m) Theory Exp.	$\delta_c \times 10^3$ (m) Theory Exp.	e_{18} Theory Exp.	$\langle\alpha\rangle$	e	Flow Dir.	Ref
1080	100	670	5.564 5.1	0.734 0.098	0.735 0.850	0.736 1.240	0.0864 0.0860	0.9975	0.1985	Down	[23]
600	100	450	3.796 3.790	0.550 0.098	0.550 0.60	0.550 2.10	0.0829 0.0880	0.9986	0.1905		
240	100	280	2.379 2.27	0.353 0.082	0.353 0.350	0.353 1.40	0.0609 0.0630	0.9996	0.1380		
1080	100	780	5.017 4.0	0.734 –	0.735 0.850	0.736 –	0.1073 –	0.9969	0.2463	Up	[24]
300	100	490	3.347 2.9	0.234 0.070	0.235 0.370	0.235 2.10	0.2168 –	0.9982	0.4990		
340	136	285	1.924 –	0.311 –	0.311 0.381	0.312 –	0.1799 –	0.9978	0.5100		[5]
227	136	235	1.562 –	0.282 –	0.282 0.300	0.282 –	0.1643 –	0.9986	0.4460		
159	136	202	1.350 –	0.234 –	0.234 0.254	0.235 –	0.1644 –	0.9990	0.4580		
454	227	512	3.873 –	0.156 –	0.156 0.318	0.158 –	0.2781 –	0.9972	0.7724		[4]

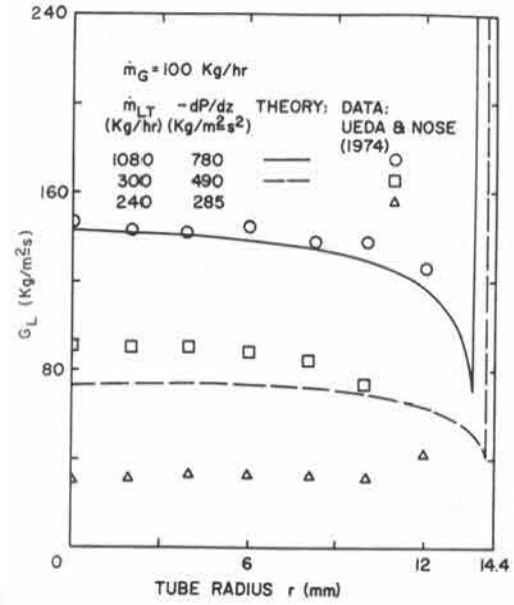

Fig. 9 Comparison of predicted liquid droplets mass fluxes in upflow with air-water data at 0.1 MPa.

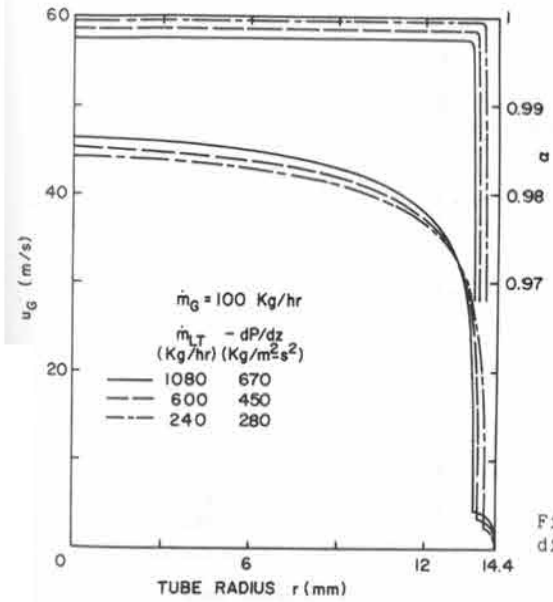

Fig. 10 Velocity and void fraction distributions in downflow.

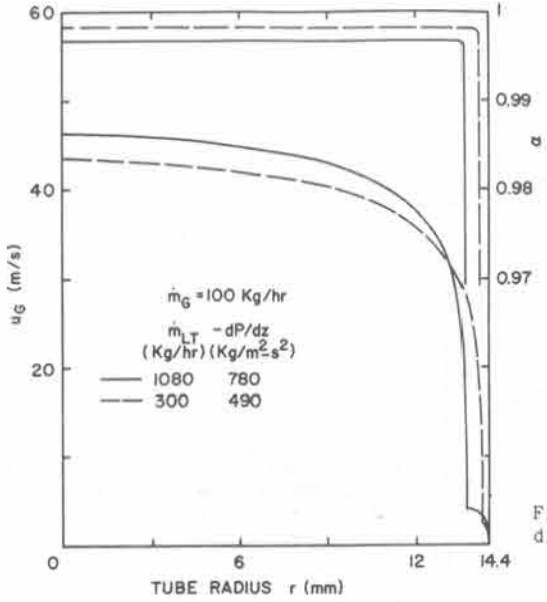

Fig. 11 Velocity and void fraction distributions in upflow.

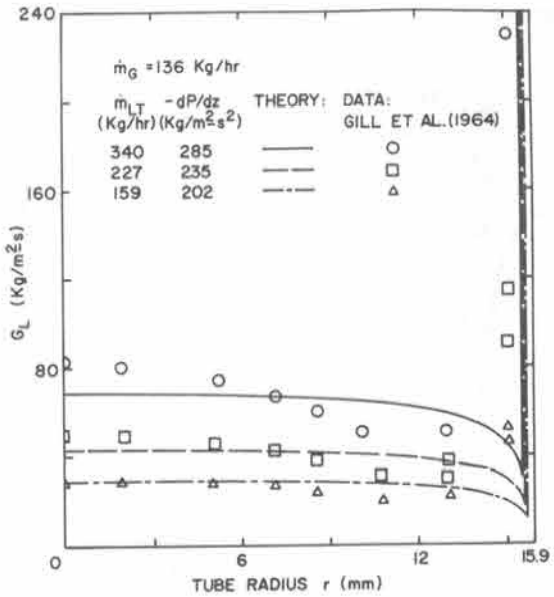

Fig. 12 Comparison of predicted liquid droplets mass fluxes in upflow with air-water data at 0.15 MPa.

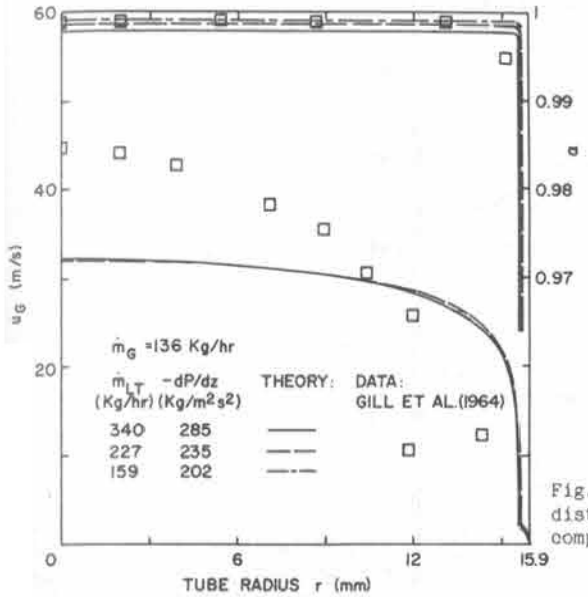

Fig. 13 Velocity and void fraction distributions in upflow and comparison with the experiment.

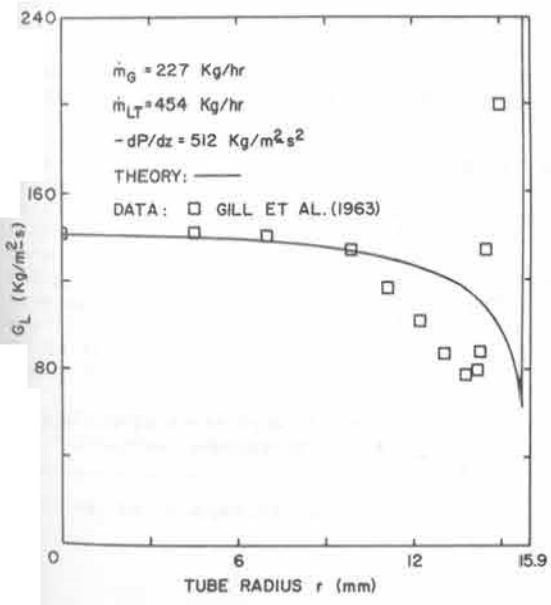

Fig. 14 Comparison of predicted liquid droplets mass flux in upflow with air-water data at 0.15 MPa.

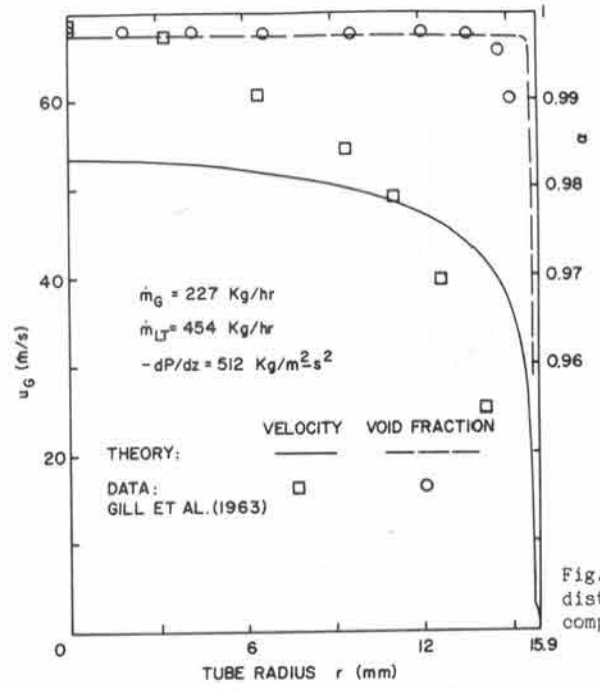

Fig. 15 Velocity and void fraction distributions in upflow and comparison with the experiment.

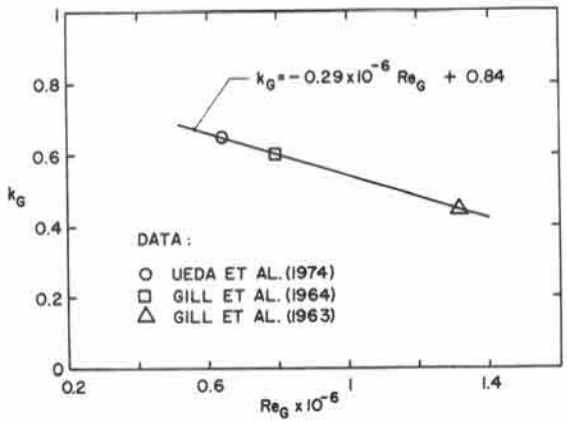

Fig. 16 Correlation of the mixing length turbulence constant.

The comparison of the predicted local liquid mass flux, core velocity, and void fraction profiles with data of Gill et al. [4] is illustrated in Figs. 14 and 15 for the situation corresponding to the gas mass flow-rate of 227 Kg/hr. Here, however, it was found that the best prediction of the data could be achieved with the mixing length turbulence constant of 0.45. On the basis of this finding we found that k_G may be correlated with the gas Reynolds number Re_G as illustrated in Fig. 16, with the best fit curve represented by the following equation:

$$k_G = -0.29 \times 10^{-6}\ Re_G + 0.84 \tag{6.1}$$

where the superficial gas Reynolds number is defined as:

$$Re_G = \frac{\rho_G \langle V \rangle D}{\mu_G} = \frac{4}{\pi} \frac{m_G}{\mu_G D} \tag{6.2}$$

All results in this paper were generated with $C_1 = 1$; i.e., the liquid phase turbulence is affected only by the gas phase turbulence. This assumption is, of course, very restrictive and should not apply at low gas mass flow-rates or high core liquid mass flow-rates, or when the droplets are larger than about 10 μm [19]. The evidence for this breakdown may also be seen in numerical calculations at low gas flow-rates where we experienced convergence difficulties and found that they could be eliminated by adjusting the parameter C_1 to a lower value. Lower values of C_1 ($C_1 < 1$) correspond to the liquid phase turbulence fluctuations of lower amplitude[4] than the gas phase as may be seen from (3.1). At the present, however, detailed annular flow data are lacking to establish the variations of k_G and C_1 at low values of m_G. The turbulence parameter k_G does not appear to depend strongly on the liquid flow-rate at higher gas flow-rates, as far as the present investigation has shown, and the correlation (6.1) appears to be adequate.

Recent experimental studies [25] in a 31.8 mm tube with an air-water upward flow clearly show that at fixed total liquid flow-rates the entrained liquid flow becomes almost independent of the gas flow-rate at high values of the gas flow, and that the liquid film is stripped of its waves. Gill et al. [5] also found that the gas core mixing length can be correlated with the gas mass flow-rate, although their definition of this constant is considerably different from the present model. The linear decrease of k_G with Re_G as shown in Fig. 16 appears to indicate that at higher gas fluxes the turbulent eddies transport their energies over shorter distances, or that the turbulent flow is more localized than at lower values of Re_G, probably due to the turbulent energy dissipation of the gas phase in the droplets or because of the reduced wave activity process. Physically, this appears to be plausible, since at lower gas flow-rates the effect of liquid film, or of the waves on the film, should be to penetrate deeper into the core region and transport with them the gas eddies over larger distances.

In comparing the model results with the experimental data use was made of the experimental values of the gas and liquid flow-rates, m_G and m_{LT}, and of

[4] This may be interpreted that the droplets are large.

the pressure gradient, $\partial P/\partial z$. For a given tube geometry, flow orientation, and fluid properties, only two of these variables are independent and a complete annular flow model should be constructed to reflect this fact. We did not pursue this approach at the outset for the reason to exclude the additional correlating parameters from analysis which would have masked the basic turbulence assumptions and, therefore, furnished us with a less uncertain range of validity of these assumptions.

7. SUMMARY AND CONCLUSIONS

An analysis of a turbulent two-phase core of an annular vertical flow was presented for the purpose of determining the core void fraction distribution. Modeling of the core turbulence characteristics was achieved by an assumption which relates the liquid phase turbulence to the gas phase turbulence, and by an assumption that the gas phase turbulence can be modeled by a mixing length theory. The additional assumption of the quasi-isotropicity of the two-phase high quality flow allowed the determination of the void fraction profiles in different regions of the core. In vertical upflow, the void fraction exhibits a peak close to the liquid film interface for some range of parameters, whereas in a vertical downflow the peak in void fraction is predicted at the pipe centerline. Upward flows at high values of the average void fraction do not appear to exhibit void fraction peaks close to the liquid film interface, as contrasted with flows at low void fractions. Larger interfacial shear at the liquid film interface is shown to increase the gas phase concentration close to the interface in both upflow and downflow and it also tends to produce larger void fraction gradients and flattening of the core void fraction profile. The results presented in the paper also compare well qualitatively with the upflow and downflow data of bubbly flows and flows without the liquid film with a denser phase dispersed in a lighter continuous phase.

Based on the experimental values of the pressure gradient, and gas and liquid mass flow-rates, the model is able to predict well the average film thickness, wall shear stress, liquid entrainment, and the detailed distribution of the liquid mass flux and void fraction in the core. This prediction is found to be more reasonable at higher values of the gas flow-rates where the mixing length constant k_G appears to exhibit a near-linear behavior with the gas flow-rate, and where the turbulence parameter $C_1=1$. At low values of m_G, the turbulence constants k_G and C_1 deviate from constant values which was attributed to the breakdown of the basic turbulence assumptions. The turbulent flow structure of an annular two-phase flow is exceedingly complex due to the presence of multiple turbulence length scales with more data required to establish the most important scales for the use in constructing realistic flow models.

NOMENCLATURE

A_1, A_2, A_3	Variables in (5.16)
Bo	Buoyancy number, $1-\rho_G/\rho_L$
C_1	Turbulence constant, defined by (3.1)
D	Tube diameter
e	Liquid droplets entrainment ratio, defined by (5.27)
$\mathbf{D}_k$	Symmetric part of the velocity gradient of phase k
f^k	Isotropicity function, defined by (3.8)
g	Gravitational constant
G	Mass flux
I	Unit tensor
k_G	Mixing length turbulence constant in (3.3)
K_G	Turbulence constant in (3.5)
ℓ_G	Mixing length in (3.3)
ℓ_o	Mixing length in (A.2)
m_G	Mass flow-rate
N_G	Parameter defined by (3.27)
N_L	Two-phase Grashof number, defined by (3.27)
p	variable defined by (A.6)
$\mathbf{p}_k$	Momentum interaction, defined by (2.5)
P	Pressure
q	Ratio of densities, ρ_L/ρ_G
Q	Parameter defined by (3.1)
r, r^+	Radial coordinate, $u_* r\rho_L/\mu_L$
R, R^+	Tube radius, $u_* R\rho_L/\mu_L$
Re_G	Gas Reynolds number, defined by (6.2)
Ri, Ri^*	Interfacial radius defined in Fig. 1, $u_* Ri\rho_L/\mu_L$
t	Time
T	Averaging time interval
$\mathbf{T}_k$	Stress tensor of phase k, defined by (2.4)
u_*, u^+	Axial velocity, u/u_*
u	Shear velocity
$\mathbf{v}_L$	Fluctuating velocity of phase k
$\mathbf{V}_k$	Velocity of phase k
$\langle V \rangle$	Superficial gas velocity
W_f^*	Nondimensional film flow rate, defined by (5.22)
Y, Y^+	Distance from the tube wall, $u_* Y\rho_L/\mu_L$
z	Axial coordinate

Greek

α	Gas volumetric fraction or void fraction
Υ	Nondimensional distance, defined by (3.34)
δ, δ^+	Parameter defined by (3.35), $u_* \delta\rho_L/\mu_L$
Δ	Parameter defined by (3.24)
Δ_{kL}	Virtual mass coefficient in (2.5)
η	Parameter defined by (3.26)
θ	Angle of tube inclination
λ_{kk}	Viscosity coefficient in (2.4)
μ_{kk}	Viscosity coefficient in (2.4)
μ_k	Viscosity of phase k
ξ	Nondimensional distance, defined by (3.23)
ξ_{kL}	Drag coefficient in (2.5)
ρ_k	Density of phase k
ρ_k	Partial density of phase k, $\alpha_k\rho_k$
σ_k	Turbulent stress tensor of phase k
τ_k	Viscous stress tensor of phase k
τ_i	Interfacial shear stress, defined by (3.21)
$\tau_{L,rz}$, τ_L	Viscous shear stress, total stress
ϕ_k	Fluctuating component of the volumetric fraction

Subscripts

c	Pertains to the film crest
e	Pertains to the entrainment
f	Pertains to the liquid film
G	Pertains to the gas phase
i	Pertains to the liquid film interface
ij	Tensor indices
k	Pertains to phase k, k=G,L
L	Pertains to the liquid phase
LT	Liquid total
m	Mean value
o	Pertains to a constant value in the core
w	Pertains to the tube wall

Special Symbols

< >	Core-averaged value
$\overline{\quad}^T$	Time averaging operator, defined by (2.7)

REFERENCES

1. Hetsroni, G. 1982 **Handbook of Multiphase Systems**, Hemisphere, New York.

2. Dobran, F. 1983 Hydrodynamic and heat transfer analysis of two-phase annular flow with a new liquid film model of turbulence. **Int. J. Heat Mass Transfer 26**, 1159-1171.

3. Dobran, F. 1985 Heat transfer in an annular two-phase flow. **J. Heat Transfer 107**, 472-476.

4. Gill, L.E., Hewitt, G.F., Hitchon, J.W., and Lacey, P.M.C. 1963 Sampling probe studies of the gas core in annular two-phase flow I. **Chem. Engng. Sci. 18**, 525-535.

5. Gill, L.E., Hewitt, G.F., and Lacey, P.M.C. 1964 Sampling probe studies of the gas core in annular two-phase flow II. **Chem. Engng. Sci. 19**, 665-682.

6. Serizawa, A., Kataoka, I., and Michiyoshi, I. 1975 Turbulence structure of air-water bubbly flow. **Int. J. Multiphase Flow 2**, 221-259.

7. Oshinowo, T., and Charles, M.E. 1974 Vertical two-phase flow, Part I, flow pattern correlations. **Can. J. Chem. Engng.** 52, 25-35.

8. Ibragimov, M. Kh., Bobkov, V.P., and Tychinski, N.A. 1973 Investigation of the behavior of the gas phase in a turbulent flow of a water-gas mixture in channels. **High Temperature 11**, 935-944.

9. Lance, M., and Bataille, J. 1983 Turbulence in the liquid phase of a bubbly air-water flow. **Advances in Two-Phase Flow and Heat Transfer**, Vol. 1, Martinus Nijhoff Publishers, 403-427.

10. Theofanous, T.G., and Sullivan, J. 1982 Turbulence in two-phase dispersed flows. **J. Fluid Mech. 116**, 343-362.

11. Drew, D.A., and Lahey, R.T. 1982 Phase distribution mechanisms in turbulent low-quality two-phase flow in a circular pipe. **J. Fluid Mech. 117**, 91-106.

12. Jeffrey, R.C., and Pearson, J.R.A. 1965 Particle motion in laminar vertical tube flow. **J. Fluid Mech. 22**, 721-735.

13. Dobran, F. 1983 A two-phase fluid model based on the linearized constitutive equations. **Advances in Two-Phase Flow and Heat Transfer**, Vol. 1, Martinus Nijhoff Publishers, 41-59.

14. Dobran, F. 1985 Theory of multiphase mixtures. **Int. J. Multiphase Flow 11**, 1-30.

15. Dobran, F. 1984 Constitutive equations for multiphase mixtures of fluids. **Int. J. Multiphase Flow 10**, 273-305.

16. Drew, D.A., and Lahey, R.T. 1977 Phase distribution mechanisms in turbulent two-phase flow in channels of arbitrary cross section. **J. Fluids Engng. 103**, 583-589.

17. Ishii, M. 1975 **Thermo-Fluid Dynamic Theory of Two-Phase Flows.** Eyrolles, Paris.

18. Dobran, F. 1984 On the formulation of conservation, balance and constitutive equations for multiphase flows. **Multiphase Flow and Heat Transfer Symposium III**, Part A, Elsevier, 23-39.

19. Hinze, J.O. 1972 Turbulent fluid and particle interaction. **Progress in Heat and Mass Transfer 6**, 433-452.

20. Tsuji, Y., Morikawa, Y., and Shiomi, H. 1984 LDV measurements of an air-solid two-phase flow in a vertical pipe. **J. Fluid Mech. 139**, 417-434.

21. Pogson, J.T., Roberts, J.H., and Waibler, P.J. 1970 An investigation of the liquid distribution in annular-mist flow. **J. Heat Transfer 92**, 651-658.

22. Laufer, J. 1954 The structure of turbulence in fully developed pipe flow. NACA Technical Report 1174.

23. Ueda, T., and Tanaka, T. 1974 Studies of liquid film flow in two-phase annular and annular-mist flow regions. Part-1, downflow in a vertical tube. **Bull. JSME 17**, 603-613.

24. Ueda, T., and Nose, S. 1974 Studies of liquid film flow in two-phase annular and annular-mist flow regions. Part-2, upflow in a vertical tube. **Bull. JSME 17**, 614-624.

25. Owen, T., and Hewitt, G.F. 1985 Data and analysis of pressure gradient and liquid entrainment in vertical annular gas-liquid flow. European Two-Phase Flow Meeting, Marchwood Engng. Lab., 4-7 June.

APPENDIX - Derivation of Equation (3.4)

In deriving (3.4) it is assumed that the addition of liquid droplets into a turbulent gas produces an additive effect on the total core turbulence, since the bubbly two-phase flow data [9,10] show that such an assumption is reasonable. For the turbulent shear stress of the gas we may write:

$$\sigma_{G,rz}(r) = \rho_G(\ell_o^2+\ell_G^2)\,\left|\frac{du_G}{dr}\right|\frac{du_G}{dr} \tag{A.1}$$

where $\ell_G=k_G(Ri-r)$ is the mixing length (equation (3.3)) and ℓ_o is a characteristic turbulent length scale of the interfacial region of the liquid film. This length may be assumed to be proportional to the thickness of Region I (see Fig. 1) or to an amplitude of interfacial waves. Comparing (A.1) and (3.2) shows that

$$\sigma_{G,Ri}(r) = \rho_G\ell_o^2\,\left|\frac{du_G}{dr}\right|\frac{du_G}{dr} = -\rho_G\ell_o^2\left(\frac{du_G}{dr}\right)^2 \tag{A.2}$$

since we expect that $du_G/dr<0$. Using the notation of $\sigma'_{G,Ri}=d\sigma_{G,Ri}/dr$, $\sigma''_{G,Ri}=d^2\sigma_{G,Ri}/dr^2$, $u'_G=du_G/dr$, and $u''_G=d^2u_G/dr^2$ we can differentiate (A.2) twice and eliminate u'_G to obtain:

$$\sigma'_{G,Ri} = 2\sigma_{G,Ri}\frac{u''_G}{u'_G} \tag{A.3}$$

$$\sigma''_{G,Ri} = \frac{1}{2\sigma_{G,Ri}}(\sigma'_{G,Ri})^2 + o(u'''_G) \tag{A.4}$$

where $o(u'''_G)$ denotes terms containing the third and higher order derivatives of the velocity profile. Expanding also $\sigma_{G,Ri}(r)$ in a Taylor series about $\sigma_{G,Ri}(Ri)$ results in

$$\sigma_{G,Ri}(r) = \sigma_{G,Ri}(Ri) + \sigma'_{G,Ri}(r-Ri) + \frac{1}{2}\sigma''_{G,Ri}(r-Ri)^2 + o(\sigma'''_{G,Ri}) \tag{A.5}$$

Ignoring the third and higher order effects of the velocity profile in (A.4) and third and higher order terms in (A.5) it is possible to combine these two equations to obtain a differential equation for

$$p = \frac{\sigma_{G,Ri}(r)}{\sigma_{G,Ri}(Ri)} \tag{A.6}$$

i.e.

$$p' = -\frac{2p}{Ri-r}\left[1 \pm p^{1/2}\right] \tag{A.7}$$

Noting that $1>p>0$ and $p'>0$, since away from the liquid film interface $\sigma_{G,Ri}(r)$ should not contribute substantially to the turbulence in the core, the physical part of (A.7) becomes

$$p' = \frac{2}{Ri-r}p^{1/2}\left[1 - p^{1/2}\right] \tag{A.8}$$

and can be integrated from $r=Ri$ where $p=1$ to $Ri>r>0$. The result is

$$p = \left(\frac{r}{Ri}\right)^2 \tag{A.9}$$